Proceedings of PRADS2016
4th – 8th September. 2016
Copenhagen. Denmark

Sloshing flows in a free surface anti roll tank - numerical simulations and experimental validation

Yue Li, Karl Henning Halse and Jiafeng Xu

Faculty of Marine Technology and Operations, NTNU, Ålesund, Norway

Abstract

Anti-roll tanks are tanks fitted onto ships in order to improve their response to roll motion, which has typically the largest amplitude among all the degrees of freedom. This paper presents a comparative study of a Volume of Fluid (VOF) based Eulerian method and a Lagrangian Smoothed Particle Hydrodynamics (SPH) method in the simulation of sloshing flow inside a free surface tank (FST). The numerical schemes of the VOF and SPH methods are outlined and the simulation results are compared as well as the computational efficiency. Both slight and violent sloshing cases are considered. All the numerical results are validated by corresponding experimental data. Through the comparison, suggestions regarding to numerical calculations in terms of accuracy and efficiency have been given. Besides, a FST sloshing regime based on frequency domain study has been proposed. The performance of the FST is fully discussed based on this regime.

Keywords

Volume of Fluid; Smoothed Particle Hydrodynamics; Free surface tank; Model test; Sloshing regime.

Introduction

The stability of a ship has always been an important topic for ensuring the safety of transportation and offshore operation. The excessive motion of a ship can seriously degrade the performance of machinery and personnel. Of all degrees of freedom, roll is the most critical one, because it is often lightly damped, in particular in the resonance range. Ship roll stabilization has therefore drew considerable attention from Naval Architects and designers.

A wide variety of roll stabilization devices have been developed over the past hundreds of years (Moaleji and Greig 2007). Anti–roll tank is considered as a simple, low cost but effective device. The basic principal of a free surface anti-roll tank is moving fluid inside the tank from starboard to port side and vice versa, with a certain phase lag with respect to the ship's roll motion. Thus, a counteracting moment is created. In some cases, additional baffles are placed inside the tank to optimize the design. Performance of a FST mainly depends on a combination effect of counteracting moment and phase lag.

A good design can greatly reduce the vessel roll motion while an improper design can be useless or even work in a negative way. Therefore, designing effective anti-roll tanks in an accurate and efficient way will definitely benefit Naval Architects and designers.

With the increase of computer resources and development of numerical algorithms, numerical simulations are playing an increasing important role in the design and optimization phase by engineers. Experiments are accompanied with simulations providing validation and a better physical understanding of fluid behavior.

In this paper, we discuss and compare two popular numerical methods: VOF based Eulerian method and SPH method in the study of free surface tanks. The kernel functions and boundary treatment of SPH is studied by X.Y.Cao and F.R. Ming (2014). They adopted dummy particles boundary and suggested that Gaussian kernel function was suitable for the sloshing study. Extensive VOF method comparative studies on sloshing loads has been made by Cariou and Casella (1999). Here we intend to compare the two methods in a more straightforward way and provide numerical suggestions based on this study. All of the numerical calculations have been validated by model tests. Besides, a FST sloshing regime based on frequency domain study has been proposed. The performance of the FST is fully discussed based on this regime.

Mathematical Formulation

The motion of fluid flow can be described in two ways. In Lagrangian description, a fluid flow field can be thought of as being comprised of a large number of finite sized fluid particles which have mass, momentum, internal energy, and other properties.

Fig. 1: Fluid description Lagrangian (left) and Eulerian (right)

Another view of fluid motion is the Eulerian description. In the Eulerian description of fluid motion, we consider how flow properties change at a fluid element that is fixed in space and time (x, y, z, t), rather than following

individual fluid particles.

The motion of a fluid can be described by a set of partial differential equations expressing conservation of mass, momentum and energy per unit volume of the fluid. The Navier Stokes equations for three dimensional compressible fluid flow can be written in conservation form as follows:

$$\begin{cases} \frac{d\rho}{dt} = -\rho\nabla\cdot\boldsymbol{v} \\ \frac{d\boldsymbol{v}}{dt} = -\frac{1}{\rho}\nabla P + \boldsymbol{\Theta} + \frac{F}{\rho} \\ \frac{de}{dt} = -\left(\frac{P}{\rho}\right)\nabla\cdot\boldsymbol{v} \\ P = (\gamma-1)e\rho \end{cases} \quad (1)$$

Where ρ is particle density; $\boldsymbol{v}$ is local particle velocity; P is pressure; $\boldsymbol{\Theta}$ is diffusion terms; F is external forces and e is the internal energy.

Finite Volume Method (FVM) is widely used in an Eulerian description. The interface between the phases of the mixture is resolved by using a simple multiphase model - Volume of Fluid (VOF) model.

VOF, introduced by Hirt and Nichols (1981), is suited to simulate flows of several immiscible fluids on numerical grids capable of resolving the interface between the phases of the mixture. The VOF model description assumes that all immiscible fluid phases present in a control volume share velocity, pressure, and temperature fields. Therefore, the same set of basic governing equations describing momentum, mass, and energy transport in a single-phase flow is solved.

The main equations are:

$$\rho = \sum_i \rho_i \boldsymbol{\alpha_i} \quad (2)$$

$$\mu = \sum_i \mu_i \boldsymbol{\alpha_i} \quad (3)$$

$$c_p = \sum_i \frac{(c_p)_i \rho_i}{\rho} \boldsymbol{\alpha_i} \quad (4)$$

Where,

$\boldsymbol{\alpha_i} = v_i/v$ is the volume fraction and ρ_i . μ_i and $(c_p)_i$ are the density, molecular viscosity and specific heat of the i th phase.

The conservation equation that describes the transport of volume fractions a_i is:

$$\frac{d}{dt}\int_V \boldsymbol{\alpha_i} dV + \int_S \boldsymbol{\alpha_i}(v - v_g)\cdot da = \int_V \left(s_{\boldsymbol{\alpha_i}} - \frac{\boldsymbol{\alpha_i}}{\boldsymbol{\rho_i}}\frac{D\boldsymbol{\rho_i}}{Dt}\right)dV \quad (5)$$

Where $s_{\boldsymbol{\alpha_i}}$ is the source or sink of the i th phase, and $D\rho_i/Dt$ is the material or Lagrangian derivative of the phase densities ρ_i.

Refer CD-adapco (2016) for further details.

SPH method based on a Lagrangian description is considered as an efficient numerical method, which is widely studied recently. By assuming the fluid is weakly compressible (i.e. density variations ≤ 1%), barotropic (i.e. $P = P(\rho)$) and polytropic(i.e. $PV^\gamma = C$), the direct relation between pressure and density can be established which is suitable for bulk flow (Batchelor 1974)

$$P_a = \frac{c_0^2\rho_0}{\gamma}\left[\left(\frac{\rho}{\rho_0}\right)^\gamma - 1\right] \quad (6)$$

c_0 is the sound speed in water; $\gamma = 7$ and the reference density $\rho_0 = 1000\ kg/m^3$.

The diffusion terms can be constructed by different approaches in SPH. In this paper, we used the artificial viscosity proposed in Monaghan (1992). The equations can be written in SPH form as

$$\begin{cases} \frac{d\rho_a}{dt} = \sum_b m_b \boldsymbol{v_{ab}}\nabla_a W_{ab} \\ \frac{d\boldsymbol{v_a}}{dt} = -\sum_b m_b\left(\frac{P_b}{\rho_b^2} + \frac{P_a}{\rho_a^2} + \Pi_{ab}\right)\nabla_a W_{ab} + g \\ P = \frac{c_0^2\rho_0}{\gamma}\left[\left(\frac{\rho}{\rho_0}\right)^\gamma - 1\right] \end{cases} \quad (7)$$

$$\boldsymbol{v_{ab}} = \boldsymbol{v_a} - \boldsymbol{v_b} \quad (8)$$

$$W_{ab} = W(\boldsymbol{x_b} - \boldsymbol{x_a}.h) \quad (9)$$

$$\Pi_{ab} = \begin{cases} -\frac{\alpha\overline{c_{ab}}\mu_{ab}}{\overline{\rho_{ab}}} & \boldsymbol{v_{ab}x_{ab}} < 0 \\ 0 & \boldsymbol{v_{ab}x_{ab}} > 0 \end{cases} \quad (10)$$

$$\mu_{ab} = \frac{h\boldsymbol{v_{ab}x_{ab}}}{\boldsymbol{x_{ab}^2} + \eta^2} \quad (11)$$

$$c_{ab} = \frac{c_a + c_b}{2} \quad (12)$$

$$\overline{\rho_{ab}} = \frac{\rho_a + \rho_b}{2} \quad (13)$$

$$\eta^2 = 0.01h^2 \quad (14)$$

α is a free parameter that can be tuned dependent on the problem.

In practice, particles are moved using XSPH variant

$$\frac{d\boldsymbol{x_a}}{dt} = \boldsymbol{v_a} + \varepsilon\sum_b \frac{m_b}{\overline{\rho_{ab}}}\boldsymbol{v_{ab}}\,W_{ab} \quad (15)$$

$$\varepsilon = 0.5 \quad (16)$$

This correction makes particle move with a velocity that is close to the average velocity in its neighborhood.

Tank Description

The free surface tank discussed in this paper is designed and to be installed on an offshore supply vessel (OSV) which is described in Table 1. Tank dimensions are initially determined based on the vessel data.

Table 1: Main dimensions of the OSV

Parameters	Value [m]
Lpp	75.5
Breadth	20
Draught	6.8
Vertical center of gravity	7.6

A very heavy tank may take a considerable amount of hull space and lower the metacentric height of the vessel and reduce its stability. Generally, the tank mass accounts for approximately 2-4% of the total ship displacement. The tank width is designed as large as possible to provide maximum damping moment. It is recommended that the designed tank length should follow:

$$L \approx 3 + 3\% \times L_{pp} \quad (17)$$

Therefore, the main dimensions are determined as shown in Table 2. Three filling levels have been considered: 33.3%, 50.0% and 66.7% respectively. The full size tank is scaled to a model size tank by a factor of 20. The model

size tank will be used in both numerical calculations and model tests. The tank motion is defined as a 1-DOF sinusoidal motion with the rotation center in the middle of the tank bottom (s=0):

$$x = A \cdot sin(\omega t) \quad (18)$$

where x is the rotating angle; A is the motion amplitude; w is rotation frequency; t is time.

Table 2: Tank dimensions

Parameters		Full-scale[m]	Model-scale[mm]
Tank width	B	20	1000
Tank length	L	5	250
Tank height	H	3	150
Filling level	h	1/1.5/2	50/75/100
Rotation point above bottom	s	0	0

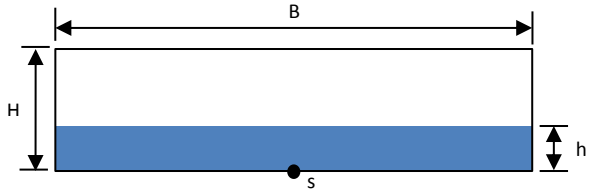

Fig. 2: Definition of geometry and tank dimensions

The following discussions including simulations and model tests are all using model scale tank.

Natural frequencies describe the modes in which a body or fluid can oscillate when excited. The relationship of any period T and frequency ω is

$$T = \frac{2\pi}{\omega} \quad (19)$$

The natural sloshing periods for a 2D rectangular tank with arbitrary water depth are given by Faltinsen and Timokha (2009).

$$T_n = 2\pi / \sqrt{\frac{\pi \cdot i}{b} g \cdot tanh\left(\frac{\pi \cdot i}{b} \cdot h\right)}.\ i = 1.2. \ldots \quad (20)$$

Where

- i is mode number;
- b is tank breadth;
- g is gravity constant;
- h is water depth;
- T1 represents the highest natural period since increasing i in the denominator of the fraction gives lower period values.

Table 3 gives a comparison between a theoretical period and calculated period from VOF simulation. The latter will be discussed in sloshing regime part.

Table 3: Natural Frequency comparison

Filling	Highest period [s]	Period from simulation [s]
33.3%	2.86	3.03
50%	2.33	2.44
66.6%	2.02	2.04

Model Test Set Up

Anti-roll tank model tests have been performed at NTNU in Ålesund. A detailed model set up is shown in Fig. 3. An angle sensor deployed at the bottom of the platform to monitor the motion of the tank. The force sensor welded on the shaft beam is to measure the force of tank and liquid, which will be converted to moment by multiplying the arm. A mirror and camera is used to capture the side view of the liquid motion. All the following numerical calculations are verified by model tests.

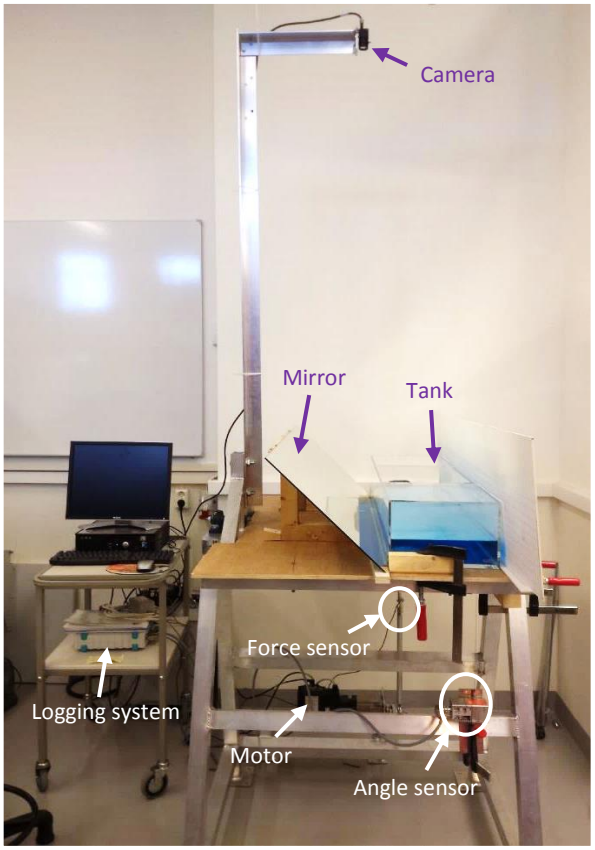

Fig. 3: Model test set up

Convergence Study

One should always ascertain that any CFD result is independent of the grid used (Roache 1997). It is necessary to find an appropriate combination of grid and time step for the following massive simulations balancing accuracy and efficiency.

Grid and time step convergence studies are done by using 2D VOF simulations. Two cases: 33% filling level, 6deg rotating amplitude, 3s and 5s excitation periods have been chosen for the study. The tank is meshed using a structured Trimmer model. Each cell inside the domain is equally treated. The boundaries around the tank are set to be no-slip smooth wall. A standard K-Epsilon turbulence model is applied to simulate the flow. The liquid is adapting a constant water density while the air inside is treated as ideal gas. The compressibility of the liquid and gas in a sloshing study has been discussed by Godderidge, et al. (2006).

In order to get the steady results, all the simulations are supposed to run for at least 20 rotating periods. However, it takes less time to enter the steady state when excited by a low frequency (e.g. excitation period is 4s or more). So we set up a global stopping criteria for 60s simulation time.

For a transient CFD calculation, it is important to maintain a low Courant number to meet the convergence requirement. The Courant number, which is the rate of flow speed with numerical disturbances propagate, should be kept below 1 in the whole computational domain while lower than 0.5 at free surface.

All the cases are calculated in the Linux CFD cluster at NTNU Ålesund, which has an Intel® Xeon® processor E5-2600 CPU. Each simulation uses 5 CPU cores. The estimated computational time for each case are listed in Table 4.

Table 4: Grid schemes for convergence study

Case	Grid Size [m] Δx	Δy	Cells	Computational time for 10s simulation
1	0.0100	0.0100	1600	0.83 h
2	0.0100	0.0050	3000	0.92 h
3	0.0050	0.0050	6000	1.27 h
4	0.0050	0.0025	12000	1.81 h

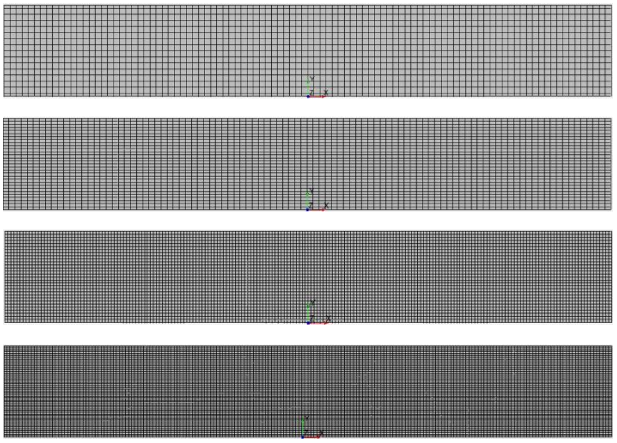

Fig. 4: Mesh with 1600 cells, 3000 cells, 6000 cells and 120000 cells for 2D simulations (from top to bottom)

Four different mesh sizes have been considered in this study. As a base case, Case1 uses a 100*16 cells domain. In top and bottom boundary layer, it uses 0.005m mesh size instead of 0.01m. Case 2 doubles the vertical cells number in Case 1 while keeping the same cells number in x direction. Case 3 uses 50% cell size than Case 1, giving a 200*30 cells domain. Similarly, Case 4 doubles the vertical cells number in Case 3. Fig. 3 gives an overview of these four mesh.

The variations of counteracting moment in time domain have been considered as the main parameter in the convergence study. Here the moment is calculated by integrating the pressure (including hydrostatic and hydrodynamic pressure) along the tank boundary.

Table 5: Grid error study - 5s excitation period

	EXP	Case 1	Case 2	Case 3	Case 4
EXP	0.00 %	5.98 %	5.18 %	5.43 %	5.04 %
Case 1		0.00 %	6.61 %	7.38 %	7.10 %
Case 2			0.00 %	1.08 %	1.21 %
Case 3				0.00 %	1.24 %
Case 4					0.00 %

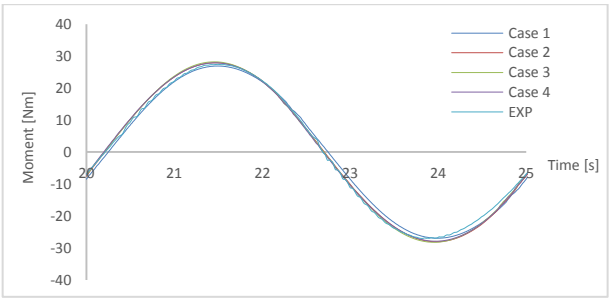

Fig. 5: Time domain moment comparison between different cells number - 5s excitation period

Fig. 5 illustrates time-domain moment curve of each case within one period. Table 5 gives a more precise variation study. We compare the relative error between each numerical calculation. From Case 1 to Case 3, the numerical difference between each case has dropped from 6.61% to 1.08% as shown in Table 5. To some extent, using finer mesh can get more stable solution. However, Case 4 has most cells of all, while it does not give much closer result to the experiments than Case 3 and Case 2. Considering its computational efficiency, Case 4 or even more cells are not recommended.

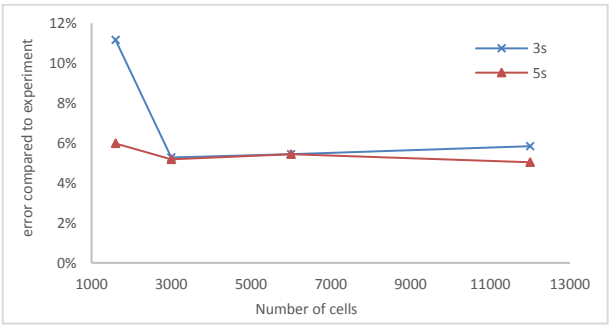

Fig. 6: Error Study – violent slosh case (3s) and slight slosh case (5s)

In Fig.6, we give the numerical error compared to experiment with respect to cells number. Both slight slosh and violent slosh cases are considered. Case 1 using the least cells can provide good results in a slight sloshing case (5s). Its performance under a more violent sloshing case (3s) however becomes worse giving more than 10% error to experiment. Although Case 1 is less time-consuming, it is less accurate than the other cases and in some situations it is even unstable.

Besides, large free surface needs a very fine grid to capture. Case 2, 3 and 4 all provide good resolution for visualization comparing to Case 1.

Overall, there is approximately 5% difference between VOF method and experiments on tank moment. From a numerical point of view, Case 2 with 100 cells in width and 30 cells in height, gives a sufficient accurate solution using relatively less time. It is the best combination of grid and computational time. However, the particles in SPH method can only accept an isotropic distance in different directions. To compare the two numerical methods, we therefore use the square mesh size (0.005m) in Case 3 for both of the numerical calculations.

Results and Discussion

Time-domain flow

Here we present a steady state flow comparison between VOF and SPH calculations. Case with 33.3% filling, 6deg amplitude, 5s excitation period is selected. Fig. 7 gives the screen shots at each second within one excitation period.

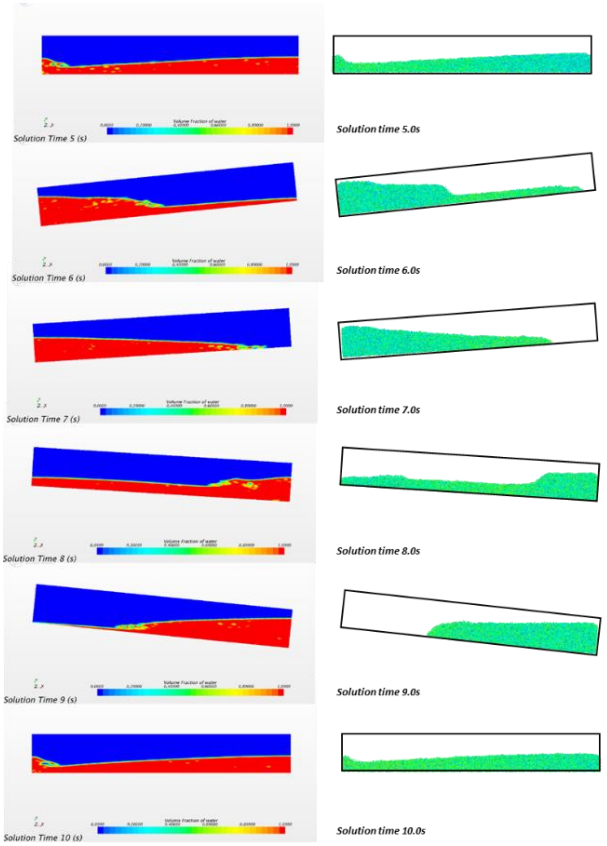

Fig. 7: Sloshing flow comparison: VOF (left) vs SPH (right)

Sloshing regime

Tank response moment and phase, the key parameters to an anti-roll tank, are obtained from the time-domain moment curve. The time-domain moment curve varies with different excitation frequencies/periods. By using Fast Fourier transform, the tank eigenfrequency and response excitation frequency can be separated.

Here we choose 7.5cm (50% filling), 3deg excitation as an example. The target time domain is from 20s to 50s avoiding the initial oscillation. Table 7 gives the peak frequency value. Small peak, which have a value less than 10% of the first peak, has been ignored. Fig. 8 shows the contribution of these two frequencies based on the frequency spectrum.

The eigenfrequency of the tank varies with the wave mode inside the tank. Based on the frequency domain study, it can be found between 0.41 and 0.45 in this case.

The dominated frequency switch from eigenfrequency to excitation frequency at the period of 1.4s.

Table 6: Frequency domain study

Excitation Period	Excitation frequency	Response Frequency First peak	Response Frequency Secondary peak
1.0	1.00	**1.00***	0.41
1.1	0.91	0.41	**0.90**
1.2	0.83	0.45	**0.83**
1.3	0.77	0.45	**0.76**
1.4	0.71	**0.72**	0.45
1.5	0.67	**0.65**	0.45
1.6	0.63	**0.62**	0.45
1.7	0.59	**0.59**	-
1.8	0.56	**0.55**	-
1.9	0.53	**0.52**	-
2.0	0.50	**0.48**	-
2.2	0.45	**0.45**	-
2.4	0.42	**0.41**	-
2.6	0.38	**0.38**	-
2.8	0.36	**0.34**	-
3.0	0.33	**0.34**	-
3.5	0.29	**0.28**	-
4.0	0.25	**0.24**	-
4.5	0.22	**0.21**	0.38
5.0	0.20	**0.21**	0.41
5.5	0.18	**0.17**	0.41
6.0	0.17	**0.17**	0.41

**value marked bold is response frequency with respect to the excitation frequency*

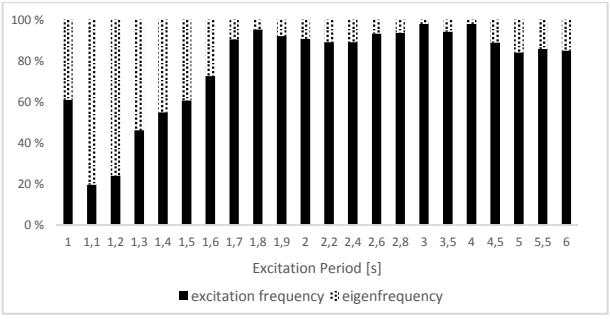

Fig. 8: Response frequency contribution

From period 1.7s to period 4.0s, only one dominated frequency (excitation frequency) can be found in the frequency domain. It indicates that the system is dominated by external excitation and enters into the damping dominate region. By using Eq. 20, the highest natural period of the tank is 2.33s (or 0.43Hz in frequency). It can be seen from the moment plot in Fig. 9 that the peak value appears between 2.2s and 2.4s. This is where the resonance occurs.

After 4.0s period, the excitation frequency starts to show up again when exceeding the damping dominated region, which indicates the system entered into an inertia dominated range. Fig. 9 illustrate a detailed division of slosh.

In the stiffness-dominated range, the tank provides very little counteracting moment to the external excitation. Flow inside has high modes. One should notice that at 1.2s, there is almost no counteracting moment. This is where the standing wave occurs.

In the inertia dominated range, liquid inside does not give a phase lag at all. This is a dangerous design range for an antiroll tank because it introduces additional negative moment to the vessel thus it may deteriorate the roll motion further.

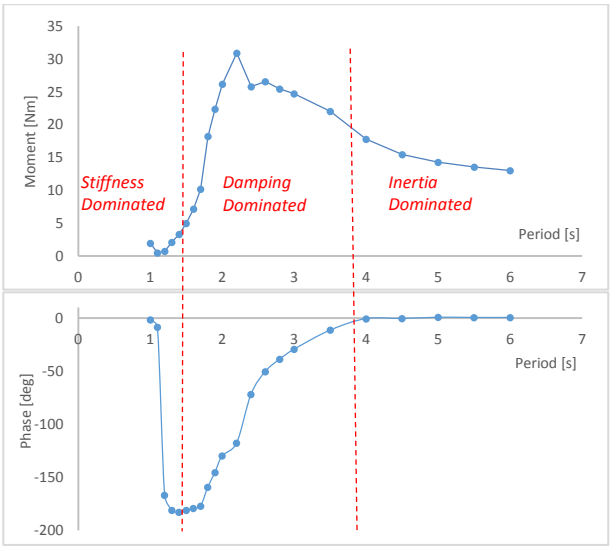

Fig. 9: Sloshing regime

For an effective anti-roll tank, one should always make sure that the tank is working in the damping range where the combination of moment and phase has positive contribution. Furthermore, the designate tank is supposed to have a -90 degree phase lag with the excitation motion to get a maximum contribution. In this case, the amplitude of the moment is approximately 30 Nm at -90deg phase.

Numerical method comparison

Strictly speaking, turbulence is a three-dimensional time-dependent phenomenon. Therefore, CFD simulations in most sloshing cases should be in three dimensions. However, a 2D simulation is computationally cheap when having same grid size. It is of interest to investigate the difference between 2D and 3D model and make proper decision for a sloshing simulation. The cell number and computational time of 2D and 3D model are compared in Table 7.

Table 7: Comparison between 2D and 3D calculations

	Cells	Computational time for 10s simulation
2D	6000	1.27 h
3D	300000	42.13 h
Ratio	1:50	1:33

2D simulation neglect the vortex in tank length direction. Besides, it does not include the effect of the tank sidewall corners. However, these two aspects may affect the result only when intense turbulent flow occurs. From the time-domain calculations shown in Fig. 10, we see that 2D case remains good consistency with 3D case at excitation period 3.0s which is considered as a violent sloshing situation. However, the difference cannot be ignored in the resonance range e.g. 2.4s excitation period.

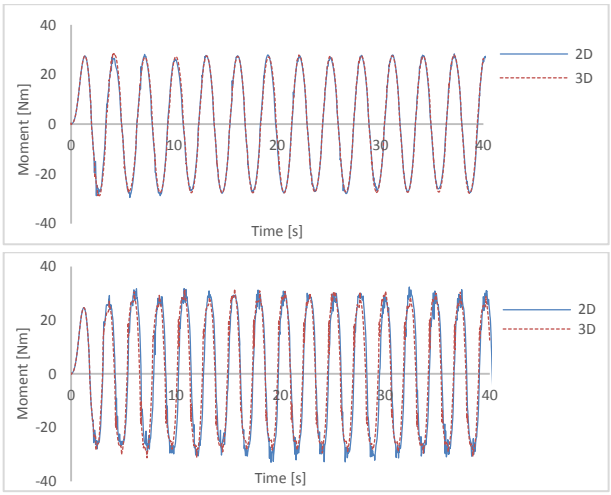

Fig. 10: Time-domain comparison between 2D and 3D at excitation period 3.0s (top) and 2.4s (bottom)

Overall, the moment differences between 2D and 3D simulations are rather small in most sloshing cases. We have confidence to argue that 2D simulations provide sufficient good result in the FST study. 3D simulations can be a validation of 2D especially when it comes to resonance range. Besides, 2D simulations are widely used in initial screening of alternative designs, and parametric studies because it is easy to implement and computationally cheap.

SPH simulations in three dimensions are calculated using CPU Intel Xeon CPU E5-2623 v3 3.00 Ghz (2 processors), GPU Nvidia GTX TITAN X GDDR5 12GB, 3072 CUDA Cores. Table 8 gives an estimated computational time for different fillings.

Table 8: Computational Time of SPH

Filling height	Particle number	Computational time for 10s simulation
5cm	132514	0.79 h
7.5cm	181269	1.08 h
10cm	230024	1.46 h

Due to the difference of computational environment, it is impossible to compare the efficiency of the two methods directly. But an impression is that SPH is able to handle a large amount of particles in a rather short time. Besides, SPH uses much less cells compared to a 3D VOF simulation as it only solve the fluid domain.

Fig 11 give a wide range of comparisons among VOF, SPH, and model tests data. The VOF simulation has shown excellent consistency with the model test in most cases. However, it over predicts the moment amplitude at resonance range. This phenomenon becomes more notable at higher filling and excitation amplitude. An explanation could be that severe tank motion results in violent slosh on free surface, which creates difficulties for the simulation.

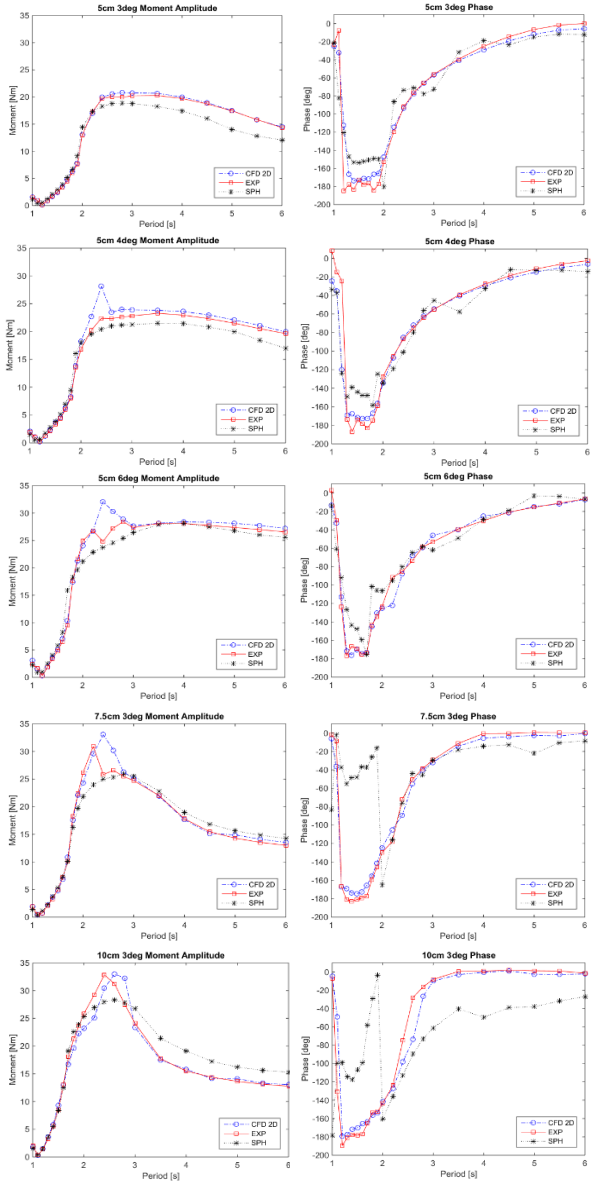

Fig. 11: Comparison among 2D CFD, SPH and Experiment

SPH method using relative less time gives excellent prediction in stiffness dominated range. It has problem to predict the resonance range. The phase angle of SPH gives insufficient accuracy, especially in higher filling levels. Further study should focus on tuning the SPH simulations.

Overall, both of the numerical simulations have shown good consistency with the model test. VOF based CFD, considered as a robust method, provides excellent result using relative long time. While SPH is a rather fast but less accurate numerical method in this slosh study. When choosing the numerical methods, one should balance both the computational time and simulation accuracy to achieve the final goal.

Excitation amplitude

In the following figures (results from model tests), the moment is expressed as moment per unit roll to make the values comparable with other amplitudes of roll. The

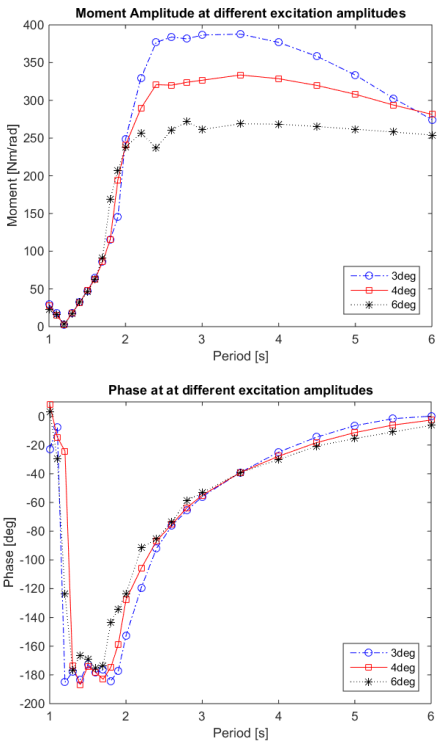

Fig. 12: Moment amplitude and phase at different excitation amplitudes

total moment can be found by multiplying with the amplitude of roll motion. When multiplying each curve by its roll amplitude, it is clear that the moment at higher excitation amplitude gives higher values than those at lower excitation amplitude.

In stiffness-dominated range, the moment amplitude has a liner increase with the excitation amplitude. However, we see a clear nonlinearity in the damping range. This trend is gradually fading when entering into the inertia-dominated range.

The bottom plot shows that the flow phase has no strong relation with the excitation amplitudes.

Filling levels

During regular operation and transportation, a ship is subjected to changes in its natural frequency. For insuring the ART effective working, one should tune the tank natural frequency to get as close as the vessel's natural frequency.

Once the main dimensions of the ART defined, changing the filling level becomes the only way to adjust the natural frequency of the tank. Here we present a study of three filling levels: 5cm, 7.5cm and 10cm, corresponding to 33.3%, 50.0% and 66.7% filling percentage.

Higher filling level has more liquid inside the tank, which gives more static force increasing the global moment. This can be found in the stiffness-dominated range.

In damping range, the flow behavior is mainly determined by the tank motion. Especially in the resonance range, the moment shows an extremely high value. Besides, the natural period of the tank reduces as the filling level increases which can also calculated by Eq. (20).

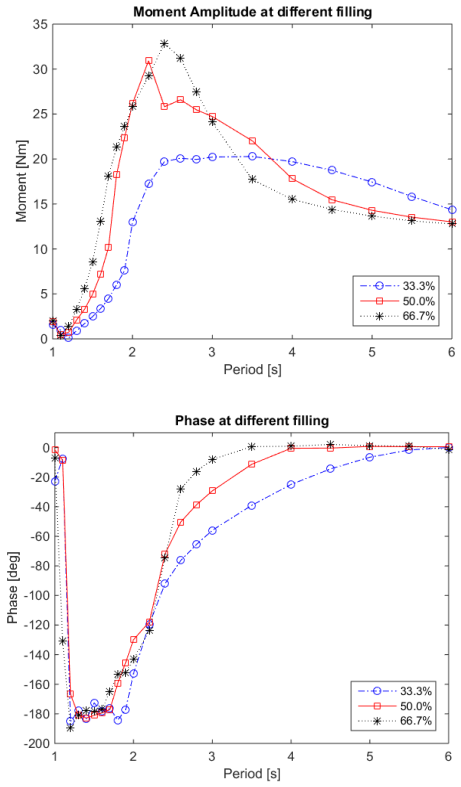

Fig. 13: Moment amplitude and phase at different filling levels

When the system enters into the inertial dominated region, the tank with more liquid however generates less moment. More liquid inside the tank gives more mass, which adds more inertial impact on the system. As it becomes more difficult to excite the liquid inside, the liquid flow moves relatively slow. Besides, the tank with more mass enters into the inertial dominated region much earlier than the tank with less mass. This can also be read from the phase curve. When the phase approaches 0 deg (after 3.0s), the system enters into the inertial dominated region.

As we know from previous analysis, ART works well only in the damping range. By comparing the phase curves, it can be found that small filling level can provide a broader damping range. Though giving less moment, a small filling tank can work in more excitation conditions. While a high filling tank can provide a high counteracting moment but in a short excitation range.

Conclusions

This paper present a comparative study of two numerical methods: a VOF based Eulerian FVM method and a Lagrangian SPH method. Both of the two methods have their own pros and cons. SPH method is efficient but lack of accuracy in some cases. While VOF provides sufficient good results but takes more time. Both of the numerical methods shows good consistency with experiments except the resonance range. One should balance the efficiency and accuracy when using these methods.

The ART sloshing regime is studied by using FFT analysis. Sloshing cases are separated by three frequency regions: stiffness, damping and inertia dominated ranges. For an effective ART, it is crucial to make sure it works in the damping dominated range. The optimized performance can be achieved at resonance range.

Besides, we study the performance of the FST at different fillings and excitation amplitudes. It has been found that moment has a clear nonlinear relation with the roll amplitude in damping region. Different excitations barely influence the flow phase. But changing the tank frequency by varying filling level has great effect on phase. Higher filling provides higher damping but in a short excitation range.

References

Batchelor, G. K. 1974. "Transport properties of two-phase materials with random structure." *Annu. Rev. Fluid Mech. 6* 227-255.

Cariou, Alain, and Guido Casella. 1999. "Liquid sloshing in ship tanks: a comparative study of numerical simulation." *Marine Structures* 12: 183-198.

Faltinsen, OM, and AN Timokha. 2009. *Sloshing.* Cambridge University Press.

Godderidge, Bernhard, Mingyi Tan, Stephen Turnock, and Chris Earl. 2006. "A Verification and Validation Study of the Application of Computational Fluid Dynamics to the Modelling of Lateral Sloshing."

Hirt, C.W., and B.D. Nichols. 1981. "Volume of Fluid (VOF) Method for the Dynamics of Free Boundaries." *Journal of Computational Physics* 39, 201.

Moaleji, and A.R. Greig. 2007. "On the Development of Ship Anti-roll Tank." *Ocean Engineering* 103-121.

Monaghan, J. J. 1992. "Smoothed particle hydrodynamics." *Annu. Rev. Astron. Astrophys.* 30: 543-574.

Roache, P J. 1997. "Quantification of uncertainty in computational fluid dynamics." *Annual Review of Fluid Mechanics* 29:123-160.

STAR-CCM+. 2016. *VOF Formulation.* User Guide, CD-adapco.

X.Y.Cao, and A.M.Zhang F.R. Ming. 2014. "Sloshing in a rectangular tank based on SPH simulation." *Ocean Engineering* 47: 241-254.